

Article

Characteristics of Aggregate Size Distribution of Nanoscale Zero-Valent Iron in Aqueous Suspensions and Its Effect on Transport Process in Porous Media

Ruiqi Duan ^{1,2,3}, Yanhui Dong ^{1,2,3,*} and Qian Zhang ^{1,2,3}

¹ Key Laboratory of Shale Gas and Geoenvironment, Institute of Geology and Geophysics, Chinese Academy of Sciences, Beijing 100029, China; drq1993@mail.iggcas.ac.cn (R.D.); zhangqian@mail.iggcas.ac.cn (Q.Z.)

² Institutions of Earth Science, Chinese Academy of Sciences, Beijing 100029, China

³ College of Earth and Planetary Sciences, University of Chinese Academy of Sciences, Beijing 100049, China

* Correspondence: dongyh@mail.iggcas.ac.cn; Tel.: +86-010-8299-8617

Received: 18 April 2018; Accepted: 15 May 2018; Published: 23 May 2018



Abstract: Bare nanoscale zero-valent iron (NZVI) particles in aqueous suspensions aggregate into micron to submicron sizes. The transport process of enlarged aggregates or multi-sized aggregates is different from that of nanoparticles. In this work, we performed aggregate size distribution analysis of NZVI suspension using a laser grain size analyzer and conducted a series of continuous injection column experiments with different injected NZVI concentrations. The results show that aggregates in NZVI suspensions range from submicron to submillimeter size and are mainly distributed around 5–9 μm and 50–100 μm . Quantitative calculation of iron transport and retention showed that the retained iron linearly correlates with injected concentration. The cross-section images revealed that clogging weakened from inlet to outlet. Furthermore, larger aggregates ($>40 \mu\text{m}$) appeared more often in the rising-declining stages of breakthrough curves, whereas small aggregates ($<30 \mu\text{m}$) dominated the steady stage. Indeed, relatively preferential flow facilitated the transport and discharge of both large and small iron aggregates. Straining of glass beads especially for the large iron aggregates resulted in a decline in breakthrough. Moreover, the blocking of attached and plugged iron prevented later retention of iron, resulting in a certain concentration of iron in the effluents. Our study provides greater insight into the transport of NZVI.

Keywords: NZVI; aggregate size distribution; multi-sized; transport

1. Introduction

Nanoscale zero-valent iron (NZVI), or iron nanoparticles, can remain as stable suspensions for long periods of time and form an in situ treatment zone when injected into groundwater. They have thus become the most attractive tool for in situ contaminated groundwater remediation owing to their large specific surface area and high reactivity with a broad range of targets such as organic compounds [1], metal ions [1,2], metalloids, and nitrates [3,4]. On the other hand, the unique size and characteristics of NZVI particles (e.g., magnetism) cause many difficulties in the groundwater remediation application of NZVI: (1) poor stability and transport in groundwater; and (2) growing particle size resulting from aggregation, and co-precipitation with products such as metal hydroxide, which leads to lowering of permeability due to clogging of pores.

The application of NZVI to in situ remediation necessitates their transport from the released point to the contaminated target zone especially for the IRZ (in situ reaction zone) technology. This requires adequate transport and stability, avoiding sedimentation and clogging halfway during transport. Previous studies mainly concentrated on the modification of NZVI with various kinds of materials, such as surfactants, to enhance its transport and stability, and involved a series of experimental and

field tests with the modified NZVI to evaluate the transport and remediation effects. Limited laboratory studies and field tests have been carried out to understand the migration of NZVI particles in a subsurface environment [5–7]. Column experiments have shown that both commercial reactive bare iron nanoparticles and modified nanoscale iron slurry (e.g., bimetal Fe-Ni particles) can penetrate porous media to less than 10 cm [8–11], while a field test in North California proved that a colloidal solution of bimetallic nanoparticles (Pd-Fe, concentration of 1.9 g/L) can migrate with water up to 6–10 m from the injected well [12]. NZVI particles tend to aggregate and sediment during transportation in the subsurface, leading to the clogging of the medium's pores and lowering of conductivity, especially in heavy metal liquids [7]. Once aqueous media are blocked by the attachment and clogging of iron, contaminated water will no longer flow through the reaction zones, thus shortening the essential contact between water and NZVI. On the other hand, a small degree of permeability reduction caused by NZVI clogging may be advantageous because of the reduced contaminant discharge and increased contact time between NZVI particles and the contaminants [13]. Therefore, it is important to investigate the characteristics and transport process of aqueous NZVI.

However, a NZVI suspension is not a stable system like colloidal solution, and the bare nanoparticles have strong magnetic attraction among themselves; thus, it is arbitrary to directly introduce the colloidal filtration theory to analyze the transport behavior. Some studies have tried to establish a linear relationship between the amount of retained iron and the injected iron concentration, simplified the relationship as experimental parameters, and applied them to existing theories (such as the colloid filtration theory [14] and the two-site colloid transport model [15,16]) to simulate the transport process of NZVI. A few research papers macroscopically described the transport process of NZVI slurry by breakthrough curves (BTCs) [5] or conductivity duration curves [7]. Considering that iron nanoparticles aggregate into submicron or micron sizes in suspensions [17], it is reasonable to take into account the effect of multi-sized aggregates when describing the detailed transport process of aqueous NZVI particles.

According to literature on NZVI, not many studies considered the effect of specific sizes of iron aggregates in different concentrations of iron suspension, but simply considered the average particle size [8,18]. However, the same suspension may contain particles and aggregates of different size ranges, which may result into a more complex transport process. In this study, the size distribution of NZVI suspension was analyzed and continuous injection column tests were performed to elucidate the transport of multi-sized iron aggregates in IRZ application from the perspective of multi-sized iron particles.

2. Materials and Methods

2.1. Material

2.1.1. Porous Media

Glass beads (Chengdu Shengtuo Instruments Ltd., Chengdu, China) were used as the porous medium for the column tests. To remove impurities absorbed on the glass beads surface and ensure stable electrochemical characteristics, the glass beads were successively treated with NaOH (0.05 mol/L), HCl (0.05 mol/L), and double-distilled water ($18.2 \Omega\text{s}^{-1}$), each procedure repeated thrice [19]. In addition, the ultrasonic dispersion method was conducted to keep the glass beads well dispersed. The glass beads were then oven-dried in a drying oven at 55 °C. The diameter of the glass grains used for suspension column tests ranged from 0.35 mm to 0.50 mm.

2.1.2. NZVI Suspension

Commercially available NZVI powder (Beijing Deke Dao King Technology Co. Ltd., Beijing, China) with an average diameter of 50 nm (Table 1) was used for the column tests. Different mass ratios of NZVI powder and tap water were mixed into nanoparticle suspensions of different concentration ranging

from 0.5 g/L to 2.5 g/L. In each test, the suspension was continuously stirred in a container to avoid gravitational settling before being injected into the column. The characteristics of tap water and final nanoparticle suspension have no significant changes in pH (7.75 to 7.92) and TDS (174 mg/L to 177 mg/L).

Table 1. Characteristics of Nanoscale zero-valent iron powder.

Product Type	Average Diameter (nm)	Purity Quotient (%)	Specific Surface Area (m ² /g)	Bulk Density (g/cm ³)	Crystal Form	Color
DK-Fe-001	50	>99.9	20	2.3	Spheroidal	Black

2.1.3. One-Dimensional Column Seepage System

An overview of the experimental setup is shown in Figure 1. The system comprised a constant-flux pump, a suspension-mixing device, a plexiglas column, and two piezometric head measurements. The mixing device included two 1 L containers, a rotor fixed at the bottom, and a piston. When tap water was pumped into the container, the piston moved downward and forced the suspension into the column. Two valves were used to ensure that the two containers worked interchangeably in the continuous injection condition. The pressures at the inlet and outlet were measured through three-way pipes, and effluents were collected from the outlet of the column at certain time. Transport tests were conducted using a column (10 cm in length and 1.0 cm in diameter) packed with dry glass beads. It is vital that the initial porosity and conductivity are maintained for each test. Thus, to avoid loss of porous medium, filter gauzes, whose mesh size was approximately equal to the diameter of the glass beads, were used at the inlet and outlet. The suspension column tests were conducted at 20 ± 2 °C.

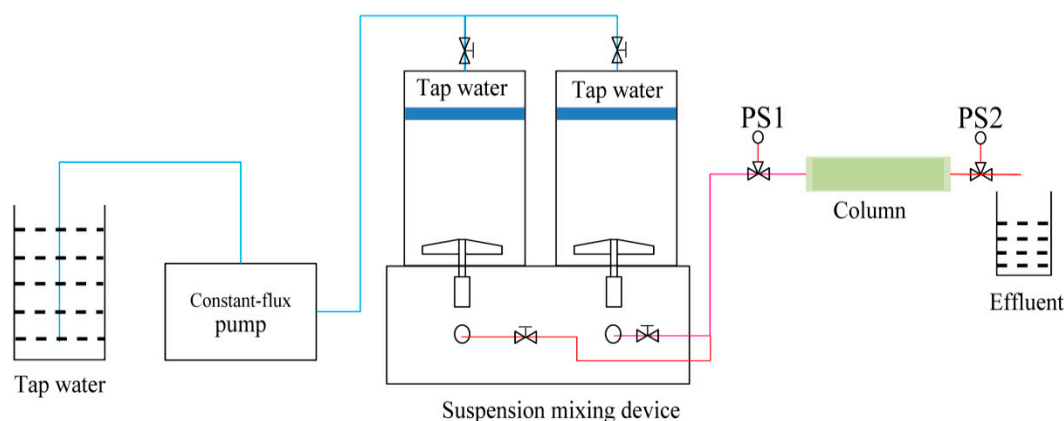


Figure 1. Schematic of column transport experiments.

2.2. Procedure of Continuous Injection Transport Tests

Continuous injection transport tests were conducted to analyze the scenario of NZVI-IRZ. The tests were carried out in a horizontal column by successively adding different concentrations of NZVI suspension. The initial porosity (n_0) was about 0.45, and the average bulk density (ρ_b) was about 1.53 g/cm³.

As is shown in Figure 1, first, tap water was injected into the container through the advection pump to maintain pressure balance, and the piston moved downward smoothly and pushed the iron nanoparticle suspension into the packed column at a constant injection rate of 10 mL/min. The valves guaranteed seamless transfer between the two vessels and enabled continuous injection. The effluents were collected at the outlet every 5 to 10 min using 2-mL centrifuge tubes and the sampling time was recorded. The parameters of the transport tests are listed in Table 2. The injection lasted for 95 min at least.

Table 2. Experimental conditions of continuous injection tests.

C_0 (g/L) ¹	V_{pore} (mL) ²	n_0 ³	ρ_b (g/cm ³) ⁴	N_{PV} ⁵	V_{sus} (L) ⁶	t (min) ⁷
0.5	3.87	0.493	1.511	306	1.01	100
1.0	3.31	0.421	1.464	317	1.05	105
1.5	3.26	0.415	1.547	291	0.95	95
2.0	3.71	0.484	1.496	256	0.95	95
2.5	3.80	0.472	1.558	255	0.97	97

¹ Injected suspension concentration (C_0); ² Pore volume (V_{pore}); ³ Initial porosity (n_0); ⁴ Bulk density (ρ_b); ⁵ Amount of injected pore volumes (N_{PV}); ⁶ Total volume of injected NZVI suspension (V_{sus}); ⁷ Injection duration (t).

2.3. Method

2.3.1. Distribution of Particle Size in NZVI Suspension

Particle size distribution of the NZVI suspension was measured using a Mastersize 3000 (Malvern Analytical Ltd., London, UK), which could detect particles ranging from 10 nm to 3500 μm . The measurements were conducted in the Key Laboratory Cenozoic Geology and Environment, Chinese Academy of Sciences.

2.3.2. Determination of Conductivity

The column was filled with glass beads and compacted to maintain the initial porosity and conductivity during successive tests. After the column was packed with glass beads, water was injected from the bottom of the vertical column to displace air upward and to ensure that the porous medium was saturated. The mass of the column before and after water injection was measured as m_1 and m_2 , respectively, and the porosity was calculated as:

$$n_0 = \frac{m_2 - m_1}{\rho_{water}}, \quad (1)$$

where ρ_{water} represents the density of water (g/cm³).

Before injecting the iron suspension, the conductivity of the column was calculated. The piezometric tubes were linked with the inlet and outlet, and the water head was measured. The water flux at the outlet was obtained by Darcy's Law:

$$K = \frac{v}{I} = \frac{Q}{AI} = \frac{Q}{A} \frac{L}{\Delta H}, \quad (2)$$

where K is the conductivity (LT⁻¹), Q is the outflow flux (L³T⁻¹), a is the cross-sectional area of the column (L²), L is the length of the seepage path (L), and ΔH is the head difference between the inlet and outlet (L).

The porosity and average density of the solid glass beads were consistent in different tests, and it is reasonable to consider that the parameters were the same.

2.3.3. Measurement of Iron Concentration

Generally, the iron content of effluent samples is measured by dissolving iron with acid. Considering the significant susceptibility of iron, a simple method has been developed and used [3,5,13]. In this study, a multi-frequency anisotropic kappameter (MFK) (Table 3) was employed to detect the iron content, and the relationship between bulk iron content and bulk susceptibility was established (Figure 2). After the completion of tests, the effluents were measured and background corrections were made to calculate the iron content.

Table 3. Parameters of MFK.

Product Type	Field Intensity (Am^{-1})	Frequency (Hz)	Sensitivity (SI)	Accuracy (%)
KLY-3S	300	967,3904, 15,616	3×10^{-8}	0.1

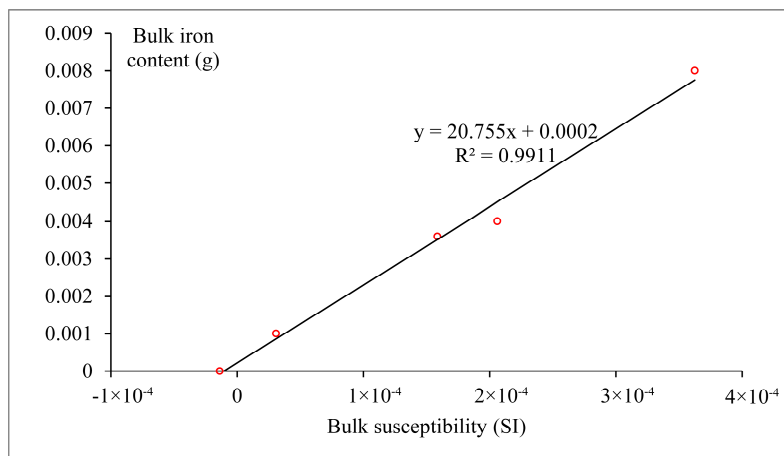


Figure 2. Relationship between iron content and susceptibility. The linear fitting relation is: $y = 20.755x + 0.0002$ with $R^2 = 0.9911$.

2.3.4. Characterization of Iron Content Profiles

For an intuitive understanding of iron retention and existence in the column, the porous media were removed from the column after every 1 cm, and the total susceptibility and mass of each part were measured; thus, the mass content of iron could be obtained. By comparing the change in iron content with the spatial profiles of different injected concentrations, the retention capacity was quantitatively evaluated. Before their removal from the column, the solid porous media (injected suspension concentration, $C_0 = 1.0$ g/L) were treated with gelatin solution to cement loose glass beads. The effect of gelatin solution flow on the iron aggregates was negligible because there was no additional pressure except for gravity. The cross sections of different parts of the column were observed and imaged using a Leica M205 a stereomicroscope (Leica Microsystems, Vienna, Austria).

2.3.5. Characterization of Iron Aggregate Size in Effluents

To evaluate the effect of multi-sized aggregates on the transport process of NZVI, the size distribution of iron aggregates was analyzed. Since the amount of effluent could not meet the shading requirements of a laser particle size analyzer, an image-based method was employed

Effluents corresponding to $C_0 = 0.5, 1.5,$ and 2.5 g/L were filtered using $0.22\text{-}\mu\text{m}$ -diameter membranes drop by drop carefully, to avoid mixing of different aggregates. Later on, the filter membranes were imaged using a stereomicroscope (Leica M205 A). The images were processed using ImageJ 1.51 to obtain the iron aggregates' size.

3. Results

3.1. Distribution of Particle Size in NZVI Suspension

The particle size distribution is shown in Figure 3. Although the commercial NZVI powder had an average size of 50 nm, aggregation occurred upon dispersion in water and the aggregate size significantly increased to the micron level. For suspensions with different concentrations, the iron aggregates can be divided into two groups according to their sizes: one group ranged from $0.5\ \mu\text{m}$ to $20\ \mu\text{m}$ for $C_0 = 0.5$ g/L and 1.0 g/L, and the other group ranged from $20\ \mu\text{m}$ to $400\ \mu\text{m}$ for $C_0 = 1.5,$ $2.0,$ and 2.5 g/L. The two low-concentration suspensions contained more aggregates no larger than

90 μm , while the three high-concentration suspensions contained a significant ratio of aggregates larger than 100 μm .

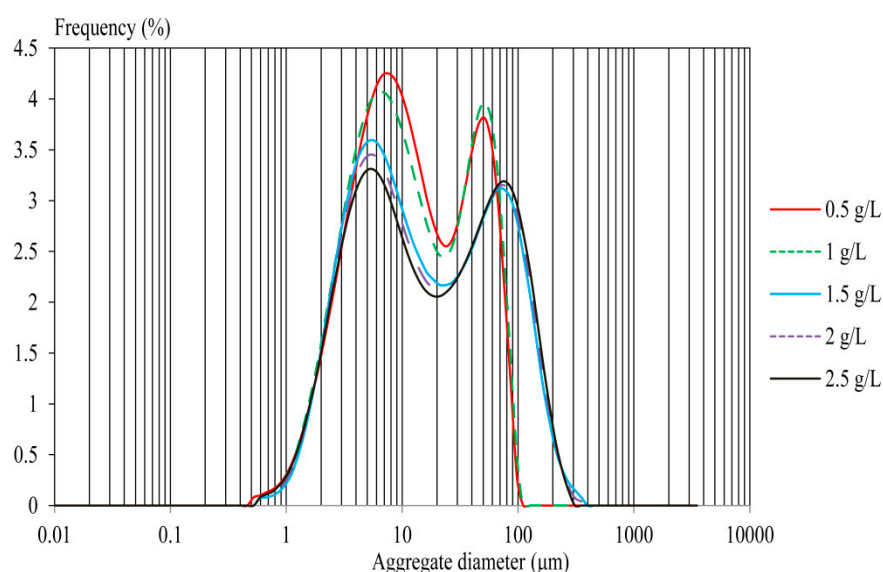


Figure 3. Particle diameter distribution of different concentrations of NZVI suspension. The horizontal axis represented iron aggregate diameter, and the vertical axis was the frequency of aggregate of different size.

3.2. Formation of NZVI Aggregates in Column

According to Schrick et al. [8], during transportation of Fe-Ni nanoparticles in sand and soil, the transport distance of the nanoparticles first increases and then decreases with increase in particle size from 30 nm to 1.2 μm . When the aggregate size is small, the effect of grain strain is limited, and iron aggregates elution is relatively easy. As size increases, interception becomes serious, and grain strain effect hinders iron aggregates with greater size from penetrating the column successfully. The impact of aggregate size on delivery of NZVI aggregates becomes obvious. The condition of $C_0 = 1.0 \text{ g/L}$ was chosen as the representative and different cross sections of the porous medium were imaged (Figure 4). As is shown in Figure 4a–c, iron aggregates are attached to or plugged the space between the glass beads near the injection point. In other words, clogging is serious and obvious. On the other hand, in Figure 4d,e, attachment of iron is dominant. Comparison of images in Figure 4 reveals that with increase in transport distance, both iron retention and clogging decreased. As is known, the larger aggregates are more likely to be intercepted and accumulate in pore spaces.

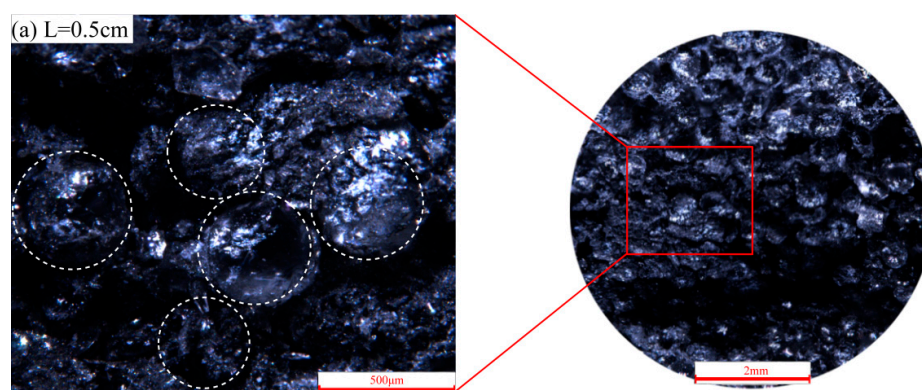


Figure 4. Cont.

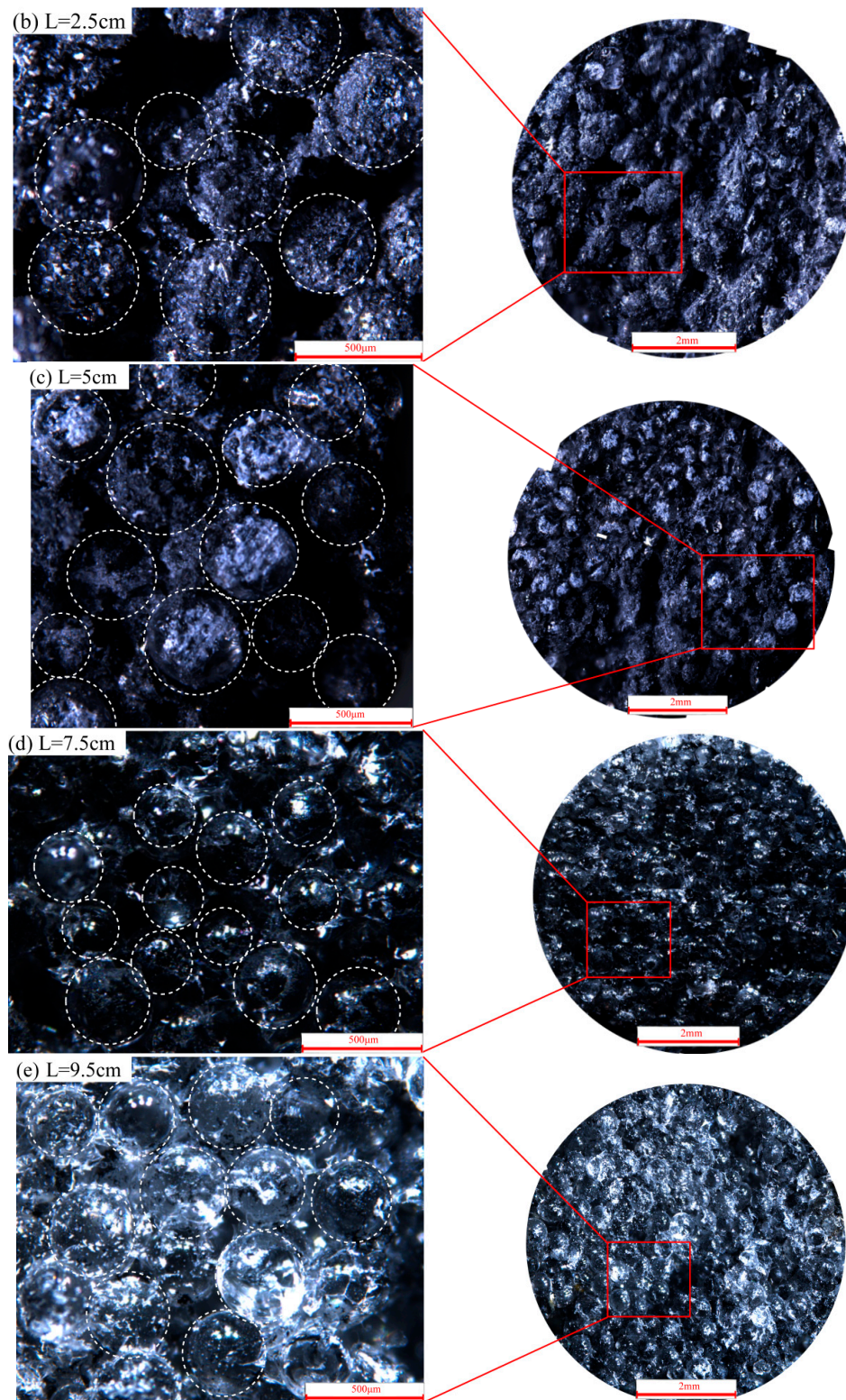


Figure 4. Iron distribution in porous media cross-sections at different column distances (L). The white dashed circles indicate porous glass beads: (a) L = 0.5 cm; (b) L = 2.5 cm; (c) L = 5 cm; (d) L = 7.5 cm; (e) L = 9.5 cm.

3.3. Spatial Iron Retention in Column

The results of iron mass content of the column, as shown in Figure 5, are consistent with those of previous studies [3,13,20]. The retained iron in the column decreased with increase in distance from the injected point. Combined with results in Figure 4, the iron aggregates not only were attached to the glass bead surface, but also clogged many pores near the injection point. As distance from the inlet increased, clogging decreased; however, attachment with the glass bead surface still existed.

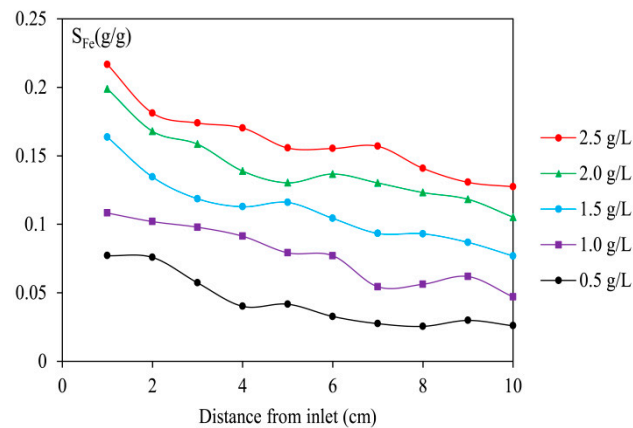


Figure 5. Iron concentration profiles along the column. S_{Fe} represents iron content per unit solid matrix, namely the mass of iron to the mass of glass beads.

3.4. Breakthrough Curves of Continuous Injection Tests

The results of the succession tests are drawn with BTCs of iron concentration (Figure 6). Compared with the results of the transport experiment of bare iron particles, which showed a migration distance of less than 7 cm and in which almost no iron particle could be detected at the outlet [8,10], the successive experiments proved that the transport of bare nanoscale iron particles is much better than expected, and a moderate amount of iron can penetrate the entire length of the column (10 cm). The BTCs were obtained under the condition of continuous injection.

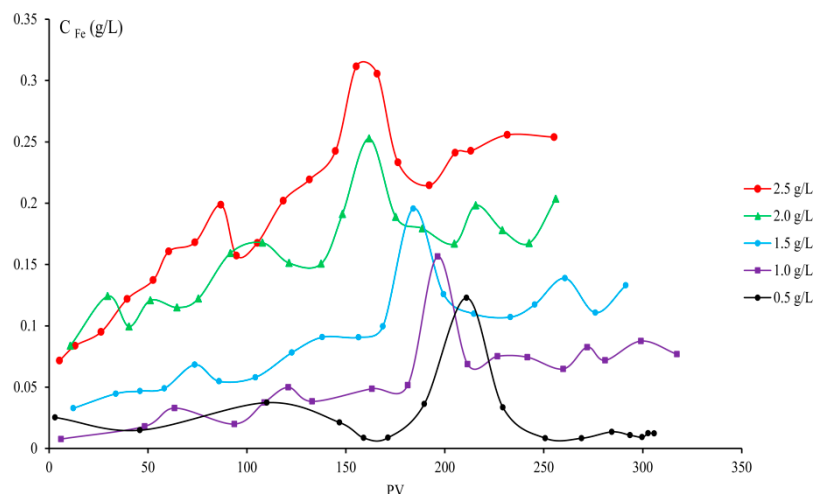


Figure 6. Breakthrough curves of iron in succession tests of different injected concentrations. PV represents pore volume, C_{Fe} represent iron concentration in the effluents. Solid points and lines in red, green, blue, purple, and black represent $C_0 = 2.5, 2.0, 1.5, 1.0,$ and 0.5 g/L, respectively.

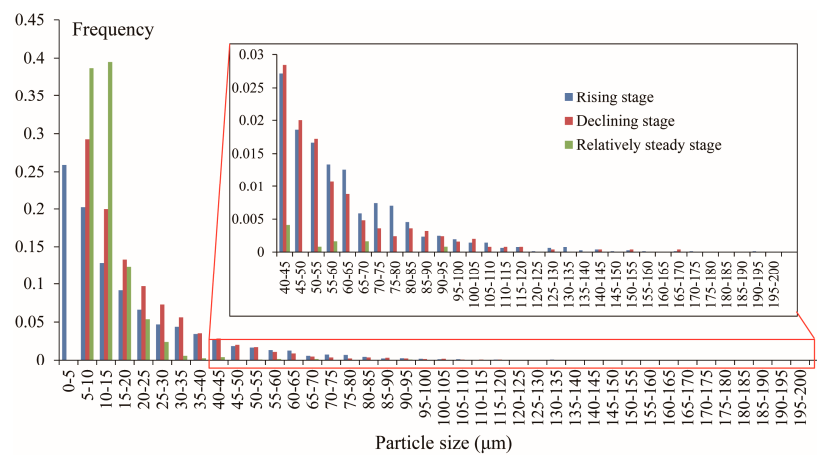
The BTCs showed a rising-declining-relatively steady stage process. Although the rising trend is reasonable for the continuous injection condition, the declining and steady stages appear abnormal. A higher concentration of injected iron led to a greater peak concentration and more iron in the effluents

3.5. Distribution of Aggregate Size in Effluents

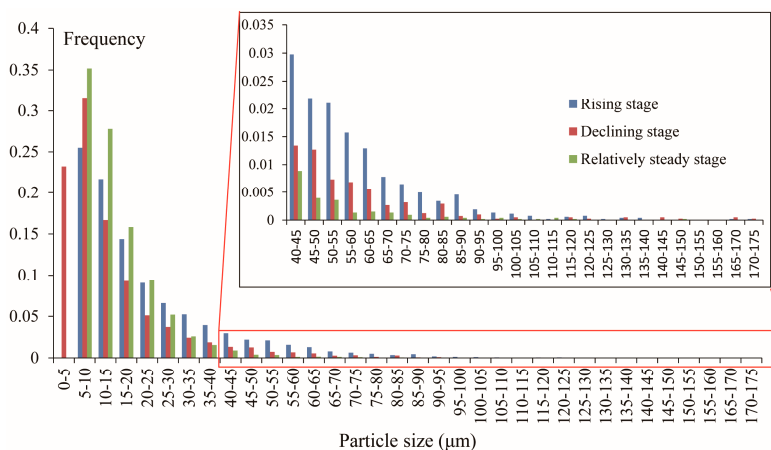
The aggregate size in effluents for different injected suspension concentrations is shown in Figure 7.

The rising and declining stages show a larger frequency than the steady stage does for diameters greater than 20 μm (the magnified graphs marked by red lines in the inset of Figure 7). The proportion of small aggregates no larger than 25 μm showed a decreasing trend (0.75 to 0.66 for the rising stage, 0.72 to 0.70 for the declining stage, and 0.96 to 0.81 for the relatively steady stage) with increase in injected concentration. In all conditions, the aggregates mainly ranged between 5 and 20 μm, especially for a low injected concentration and relatively steady stage.

Thus, it can be summarized that, in the rising and declining stages, more large aggregates (larger than 25 or 30 μm) are expelled, while in the relatively steady stage, small particles (usually less than 20 μm) can be collected.

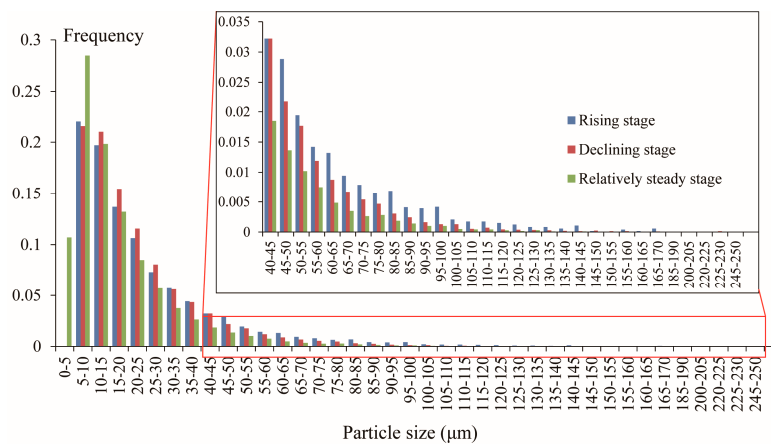


(a) $C_0 = 0.5 \text{ g/L}$



(b) $C_0 = 1.5 \text{ g/L}$

Figure 7. Cont.



(c) $C_0 = 2.5 \text{ g/L}$

Figure 7. Iron aggregate size in effluents for different injected concentrations: (a) $C_0 = 0.5 \text{ g/L}$; (b) $C_0 = 1.5 \text{ g/L}$; (c) $C_0 = 2.5 \text{ g/L}$.

4. Discussion

4.1. Quantitative Evaluation of NZVI Aggregate Retention and Transport

The iron content decreased as the distance from the inlet increased. From the BTCs (Figure 6) and iron content profiles (Figure 5), the retention and delivery of iron in the column can be quantitatively evaluated.

The mass balance of iron indicated that a significant loss of iron occurred, and larger concentrations tended to cause a greater loss (Φ_3 in Table 4). The amount of iron penetrating the column was a small fraction (Φ_1) of the total iron injected into the column (approximately 6% to 11%), and over 90% of iron remained in the column (Φ_3).

Table 4. Amount of iron retained in column and effluents, and mass loss.

$C_0 \text{ (g/L)}$	PV	$M_{Fe-out} \text{ (g)}^1$	$\Phi_1 \text{ (%) }^2$	$S_{Fe} \text{ (g)}^3$	$\Phi_2 \text{ (%) }^4$	$M_{Fe-Act} \text{ (g)}^5$	$\Phi_3 \text{ (%) }^6$	$M_{Fe-Loss} \text{ (g)}^7$
0.5	305.8	0.028	6.025	0.434	93.975	0.461	92.291	0.044
1.0	317.2	0.055	6.678	0.775	93.322	0.831	83.071	0.219
1.5	291.4	0.085	7.135	1.100	92.865	1.184	78.965	0.241
2.0	256.1	0.147	9.450	1.408	90.550	1.554	77.731	0.346
2.5	255.3	0.193	10.732	1.609	89.268	1.802	72.091	0.623

¹ The mass of iron in total effluents (M_{Fe-out}); ² The ratios of M_{Fe-out} to M_{Fe-Act} (Φ_1); ³ The mass of iron in total effluents and that retained in the column (S_{Fe}); ⁴ The ratios of S_{Fe} to M_{Fe-Act} (Φ_2); ⁵ The sum of M_{Fe-out} and S_{Fe} , namely the actual amount of iron that was injected into the column (M_{Fe-Act}); ⁶ The ratio of M_{Fe-Act} to the total iron mass in suspension (Φ_3); ⁷ The mass of iron loss during injection ($M_{Fe-Loss}$).

Both retained iron (S_{Fe}) and discharged iron (M_{Fe-OUT}) (Figure 8) show a linear positive correlation with the injected concentration (C_0). In previous studies [3], the linear relationship between the amount of attached iron and injected iron concentration were fitted with the formula obtained from the colloid filtration theory or the two-site colloidal transport model. The quantitative calculation results revealed that the retained iron (including attachment and straining) was linearly correlated with the injected iron concentration.

According to the results, the transport process of iron aggregates was accompanied with porosity decrease and permeability reduction of porous medium. In the application of NZVI in PRBs or IRZs, the remediation efficiency is directly influenced by the mobility of NZVI aggregates with different behavior, different transport distance, or mobility. It is important to control the range of iron aggregates' size to ensure the best efficiency. From this point, the relationship between aggregate size and transport

process is of importance and provides valuable information for material manufacture of bare NZVI or modified NZVI materials.

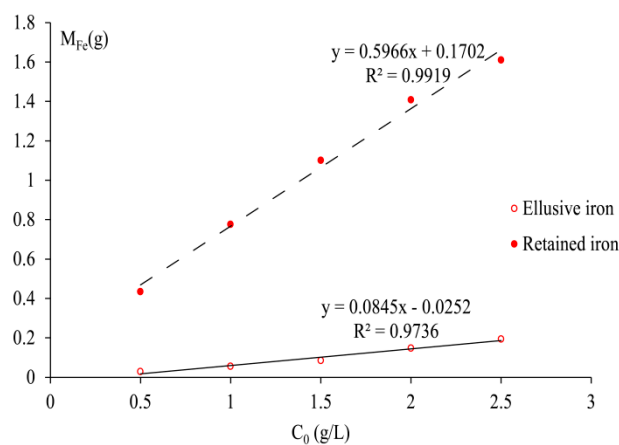


Figure 8. Relationship between residual iron and discharged iron versus initial injected concentration.

4.2. Transport Process of Iron Aggregates

The successive experiments of continuous injection (Figure 6) proved that the transport of bare nanoscale iron particles is much better than that observed in the sedimentation experiments, and BTCs can be obtained under the condition of continuous injection. Additionally, the continuous injection condition showed that attachment and clogging occurred along with blocking of the pores. The BTCs reflect the rising-declining-steady stage evolution history and can be divided into three stages.

Attachment and straining dominated the first stage. Although the glass beads are a homogeneous medium, preferential flow occurred when the aggregates traveled into column with water. It is understandable that larger pores are more attractive, especially to larger aggregates, owing to lower resistance. When a large pore was filled with many small particles, the probability of interception of the later aggregates increased. Although the larger pores were increasingly plugged, many aggregates could penetrate the column, resulting in the rising trend of the BTCs.

Under the same condition, a larger aggregate was more likely to be excluded by glass beads, with greater chances of sedimentation before traveling into the column. As the injection continued, the original large pores became smaller, and iron aggregates were forced to flow into the smaller pores, resulting in straining of the larger aggregates (maybe larger than 40–70 μm) in the column even at the inlet, which resulted in a decline in the BTCs. Thus, it could be concluded that there are more large iron aggregates in rising stage than declining stage of BTCs.

Furthermore, with increasing accumulation of iron aggregates around the matrix, blocking began to play an important role, leading to the successful escape of some small iron aggregates (no larger than 30 μm) from attachment and straining, which then penetrated the entire length of the column. This can be confirmed by the aggregate distribution results of the effluents shown in Figure 6.

Finally, residual iron and glass beads comprised a new porous system, which allowed the penetration of certain small iron particles, and the outflow of iron became steady. These trends are in good agreement with the results of Darlington et al. [21]. The difference was that, in the former study, the iron concentration gradually decreased to a very low level, which may be attributed to the difference in the porous medium employed, i.e., quartz sand and glass beads. The glass beads have smoother surfaces and weaker delivery resistance, and thus allow the transport of more aggregates.

It also can be seen from Figure 4 that a higher injected concentration tended to cause a higher peak value and a shorter rising duration. This phenomenon is reasonable because a higher concentration contains more iron aggregates of different sizes and enables the transport of more aggregates.

It is noteworthy that colloid particle size can affect dispersivity [22]. In our experiments, the suspensions did have multi-sized particles, but the distribution of iron aggregate size was similar for each suspension of different concentration. Thus, the effect of particle size on dispersivity was also similar for each test, and the BTCs were mainly controlled by the mechanism discussed above.

5. Conclusions

This study focused on the transport of bare NZVI particles in a porous medium and investigated the relationship between iron particle size and its transport capacity. The size distribution of iron in different concentrations showed that serious aggregation occurred and two groups of different size ranges of 4–9 μm and 30–70 μm , respectively. The transport of iron suspension was a comprehensive effect of the two main aggregate sizes. The BTCs showed that a moderate amount of iron could travel more than 10 cm, which was far longer than expected. Although attachment and clogging limited the delivery of bare iron particles, many particles including small and large aggregates could penetrate the column. When the iron concentration of the effluents increased to a peak value, clogging became obvious and breakthrough began to decline. Then, blocking resulted in a relatively steady outflow of bare iron, which mainly comprised small particles.

Quantitative calculation of retained iron and discharged iron according to the BTCs and column profiles revealed the iron spatial distribution. A higher injected concentration led to greater retention and discharged iron, as well as greater loss of iron.

The column profile cross-section images showed that clogging mainly occurred near the injection point, and iron aggregates were attached to the glass beads at the exit point. The analysis of aggregate distribution in the effluents showed that both large and small iron aggregates were included in the rising and declining stages of breakthrough, while the relatively steady stage mainly consisted of small aggregates. These findings provided evidence to understand the relationship between iron aggregate size and the transport process.

Although this paper focuses on the effect of injected suspension concentration on the transport of NZVI aggregates and the evolution of conductivity and porosity, it is reasonable that many other factors such as the injection rate or velocity, diameter and properties of the porous medium, and the ionic strength of the suspension should not be neglected. Therefore, it is imperative that we improve and modify the experiments and governing equations in our future work to afford a better description and simulation of NZVI transport in porous media.

In an actual porous groundwater environment, attachment and clogging/aggregation of nanoscale iron tend to be more serious, and the transport behavior is more complex because of heterogeneity. Thus, it is urgent to understand in depth the transport of NZVI aggregates in relatively simple porous media and analogically predict the delivery in natural complicated conditions.

Author Contributions: R.D. performed the experiments, and wrote the paper; Y.D. designed the experiments, offered significant advice on analysis tools and methods; Q.Z. helped in the data process and paper writing process.

Funding: This work was financially supported by the Natural Science Foundation of Beijing (Grant No. 8162042 and No. 8174077), the Strategic Priority Research Program of Chinese Academy of Sciences (Grant No. XDB10030601) and the Youth Innovation Promotion Association, Chinese Academy of Sciences (Grant No. 2016063).

Acknowledgments: We are grateful to Xuelei Feng and Beixiu Huang for their significant support during experimental work. We are grateful to the anonymous reviewers for their constructive comments and suggestions that greatly improved the manuscript.

Conflicts of Interest: The authors declare no conflict of interest.

References

1. Gillham, R.W.; O'Hannesin, S.F. Enhanced Degradation of Halogenated Aliphatics by Zero-Valent Iron. *Groundwater* **1994**, *32*, 958–967. [[CrossRef](#)]
2. Kim, S.A.; Kamala-Kannan, S.; Lee, K.-J.; Park, Y.-J.; Shea, P.J.; Lee, W.-H.; Kim, H.-M.; Oh, B.-T. Removal of Pb(II) from aqueous solution by a zeolite–nanoscale zero-valent iron composite. *Chem. Eng. J.* **2013**, *217*, 54–60. [[CrossRef](#)]
3. De Boer, C.V. *Transport of Nano Sized Zero Valent Iron Colloids during Injection into the Subsurface*; Uni Stuttgart—Universitätsbibliothek: Stuttgart, Germany, 2012.
4. Yan, W.; Lien, H.-L.; Koel, B.E.; Zhang, W.-X. Iron nanoparticles for environmental clean-up: Recent developments and future outlook. *Environ. Sci. Process. Impacts* **2013**, *15*, 63–77. [[CrossRef](#)] [[PubMed](#)]
5. De Boer, C.; Braun, J. *Characteristics and Mobility of Zero-Valent Nano-Iron in Porous Media*; University of Utrecht: Utrecht, the Netherlands, 2007.
6. Vecchia, E.D.; Luna, M.; Sethi, R. Transport in porous media of highly concentrated iron micro- and nanoparticles in the presence of xanthan gum. *Environ. Sci. Technol.* **2009**, *43*, 8942–8947. [[CrossRef](#)] [[PubMed](#)]
7. Fronczyk, J.; Pawluk, K. Hydraulic performance of zero-valent iron and nano-sized zero-valent iron permeable reactive barriers—Laboratory test. *Ann. Wars. Univ. Life Sci. SGGW Land Reclam.* **2014**, *46*. [[CrossRef](#)]
8. Schrick, B.; Hydutsky, B.W.; Blough, J.L.; Mallouk, T.E. Delivery vehicles for zerovalent metal nanoparticles in soil and groundwater. *Chem. Mater.* **2004**, *16*, 2187–2193. [[CrossRef](#)]
9. Saleh, N.; Sirk, K.; Liu, Y.; Phenrat, T.; Dufour, B.; Matyjaszewski, K.; Tilton, R.D.; Lowry, G.V. Surface Modifications Enhance Nanoiron Transport and NAPL Targeting in Saturated Porous Media. *Environ. Eng. Sci.* **2006**, *24*, 45–57. [[CrossRef](#)]
10. Tiraferri, A.; Sethi, R. Enhanced transport of zerovalent iron nanoparticles in saturated porous media by guar gum. *J. Nanopart. Res.* **2008**, *11*, 635–645. [[CrossRef](#)]
11. Tehrani, M.R.F.; Shamsai, A.; Vossughi, M. Experimental investigation of nano zero-valent iron mobility in porous media. *Sci. Iran.* **2015**, *22*, 1346–1356.
12. Glazier, R.; Venkatakrisnan, R.; Gheorghiu, F.; Walata, L.; Nash, R.; Zhang, W.-X. Nanotechnology takes root. *Civ. Eng. Fract. Mech.* **2003**, *73*, 64–69.
13. Strutz, T.J.; Hornbruch, G.; Dahmke, A.; Kober, R. Influence of permeability on nanoscale zero-valent iron particle transport in saturated homogeneous and heterogeneous porous media. *Environ. Sci. Pollut. Res. Int.* **2016**, *23*, 17200–17209. [[CrossRef](#)] [[PubMed](#)]
14. Kamai, T.; Nassar, M.K.; Nelson, K.E.; Ginn, T.R. Colloid filtration prediction by mapping the correlation-equation parameters from transport experiments in porous media. *Water Resour. Res.* **2015**, *51*, 8995–9012. [[CrossRef](#)]
15. Cullen, E.; O'Carroll, D.M.; Yanful, E.K.; Sleep, B. Simulation of the subsurface mobility of carbon nanoparticles at the field scale. *Adv. Water Resour.* **2010**, *33*, 361–371. [[CrossRef](#)]
16. O'Carroll, D.; Sleep, B.; Krol, M.; Boparai, H.; Kocur, C. Nanoscale zero valent iron and bimetallic particles for contaminated site remediation. *Adv. Water Resour.* **2013**, *51*, 104–122. [[CrossRef](#)]
17. Phenrat, T.; Saleh, N.; Sirk, K.; Tilton, R.D.; Lowry, G.V. Aggregation and sedimentation of aqueous nanoscale zerovalent iron dispersions. *Environ. Sci. Technol.* **2007**, *41*, 284–290. [[CrossRef](#)] [[PubMed](#)]
18. Tobias, R. *Particle Clogging in Porous Media*; SKB TR-10-22; Swedish Nuclear Fuel and Waste Management Co.: Stockholm, Sweden, 2010.
19. Kumar, N.; Labille, J.; Bossa, N.; Auffan, M.; Doumenq, P.; Rose, J.; Bottero, J.Y. Enhanced Transportability of Zero Valent Iron Nanoparticles in Aquifer Sediments: Surface Modifications, Reactivity, and Particle Traveling Distances. *Environ. Sci. Pollut. Res.* **2017**, *24*, 9269–9277. [[CrossRef](#)] [[PubMed](#)]
20. Strutz, T.J.; Hornbruch, G.; Dahmke, A.; Kober, R. Effect of injection velocity and particle concentration on transport of nanoscale zero-valent iron and hydraulic conductivity in saturated porous media. *J. Contam. Hydrol.* **2016**, *191*, 54–65. [[CrossRef](#)] [[PubMed](#)]

21. Darlington, T.K.; Neigh, A.M.; Spencer, M.T.; Guyen, O.T.; Oldenburg, S.J. Nanoparticle characteristics affecting environmental fate and transport through soil. *Environ. Toxicol. Chem.* **2009**, *28*, 1191–1199. [[CrossRef](#)] [[PubMed](#)]
22. Chrysikopoulos, C.V.; Katzourakis, V.E. Colloid particle size-dependent dispersivity. *Water Resour. Res.* **2015**, *51*, 4668–4683. [[CrossRef](#)]



© 2018 by the authors. Licensee MDPI, Basel, Switzerland. This article is an open access article distributed under the terms and conditions of the Creative Commons Attribution (CC BY) license (<http://creativecommons.org/licenses/by/4.0/>).